SPECIAL
Connecting the Tropics to the Polar Regions
COLLECTION

Simulating the Mutual Forcing of Anomalous High Southern Latitude Atmospheric Circulation by El Niño Flavors and the Southern Annular Mode*

AARON B. WILSON

Polar Meteorology Group, Byrd Polar and Climate Research Center, The Ohio State University, Columbus, Ohio

DAVID H. BROMWICH

Polar Meteorology Group, Byrd Polar and Climate Research Center, and Atmospheric Sciences Program, Department of Geography, The Ohio State University, Columbus, Ohio

KEITH M. HINES

Polar Meteorology Group, Byrd Polar and Climate Research Center, The Ohio State University, Columbus, Ohio

(Manuscript received 19 May 2015, in final form 28 December 2015)

ABSTRACT

Numerical simulations using the National Center for Atmospheric Research Community Atmosphere Model (CAM) are conducted based on tropical forcing of El Niño flavors. Though these events occur on a continuum, two general types are simulated based on sea surface temperature anomalies located in the central (CP) or eastern (EP) tropical Pacific. The goal is to assess whether CAM adequately represents the transient eddy dynamics associated with each of these El Niño flavors under different southern annular mode (SAM) regimes. CAM captures well the wide spatial and temporal variability associated with the SAM but only accurately simulates the impacts on atmospheric circulation in the high southern latitudes when the observed SAM phase is matched by the model. Composites of in-phase (El Niño–SAM−) and out-of-phase (El Niño–SAM+) events confirm a seasonal preference for in-phase (out of phase) events during December–February (DJF) [June–August (JJA)]. Modeled in-phase events for both EP (during DJF) and CP (during JJA) conditions support observations of anomalous equatorward momentum flux on the equatorward side of the eddy-driven jet, shifting this jet equatorward and consistent with the low phase of the SAM. Out-of-phase composites show that the El Niño–associated teleconnection to the high southern latitudes is strongly modulated by the SAM, as a strong eddy-driven jet is well maintained by high-latitude transient eddy convergence despite the tropical forcing. A regional perspective confirms that this interaction takes place primarily over the Pacific Ocean, with high-latitude circulation variability being a product of both tropical and high-latitude forcing.

1. Introduction

The southern annular mode (SAM), the dominant mode of atmospheric circulation variability in the Southern Hemisphere (SH), has been identified in numerous variables, including mean sea level pressure (MSLP), geopotential height, and zonal wind (e.g., Rogers and van Loon 1982; Karoly 1990; Kiladis and Mo 1998; Gong and Wang 1999; Thompson and Wallace 2000; Simmonds and King 2004). The SAM represents oscillations in atmospheric mass between the mid- and high latitudes and thus the meridional variability of the circumpolar westerly winds. The SAM varies from daily (Baldwin 2001) to interdecadal time scales (Kidson 1999) and can occur without external forcing (Limpasuvan and Hartmann 1999, 2000). The persistence and internal variability of the SAM is the result of positive feedbacks between baroclinicity and the meridional propagation of high-frequency eddies in the upper levels of the atmosphere, such that the Ferrel cell maintains a strong thermal gradient near the eddy-driven jet that perpetuates its displacement (e.g., Karoly 1990; Yu and Hartmann 1993;

*Byrd Polar and Climate Research Center Contribution Number 1541.

Corresponding author address: Aaron B. Wilson, Byrd Polar and Climate Research Center, The Ohio State University, 1090 Carmack Rd., Columbus, OH 43210.
E-mail: wilson.1010@osu.edu

DOI: 10.1175/JCLI-D-15-0361.1

Hartmann and Lo 1998; Hall and Visbeck 2002; Rashid and Simmonds 2004, 2005; Kidston et al. 2010). On intermediate time scales, thermal feedbacks between the ocean and atmosphere maintain SAM-induced anomalies of surface temperature and sea ice for weeks or months beyond the initial atmospheric signal (Sen Gupta and England 2006; Ciasto and Thompson 2008). Late twentieth-century trends toward a high-polarity SAM have been linked to decreases in stratospheric ozone over Antarctica with propagating effects into the troposphere during austral summer (e.g., Thompson and Solomon 2002; Gillett and Thompson 2003; Thompson et al. 2011), as well as increasing greenhouse gases (Fyfe et al. 1999; Kushner et al. 2001; Marshall et al. 2004; Simpkins and Karpechko 2012; Zheng et al. 2013).

Low-frequency forcing of the atmospheric circulation in the SH is also tied to the atmosphere–ocean coupled El Niño–Southern Oscillation (ENSO) (Trenberth 1997). During the warm phase of ENSO (El Niño), a weakening/reversal of the tropical trade winds allows anomalous warm water to move toward the central and/or eastern equatorial Pacific Ocean, shifting tropical convection eastward and affecting global atmospheric circulation (Hoskins and Karoly 1981; Arkin 1982). The ENSO teleconnection to the SH is characterized as a Rossby wave, specifically the Pacific–South American pattern (PSA) (e.g., Mo and Ghil 1987), displayed as alternating positive and negative geopotential height anomalies extending from the west central equatorial Pacific Ocean toward the South Pacific Ocean near the Amundsen–Bellingshausen Seas (ABS) region. This teleconnection is most evident during SH winter (Karoly 1989), as El Niño creates high-pressure ridging in the ABS (Renwick 1998; Renwick and Revell 1999; Revell et al. 2001). Rossby waves depend on the spatial distribution of the deep convection in the central equatorial Pacific (Mo and Peagle 2001; Harangozo 2004; Lachlan-Cope and Connolley 2006), with location and intensity being the key forcing for the high-latitude blocking events.

Dynamically, Seager et al. (2003) described a mechanism different from the Rossby wave interaction on SH circulation whereby an El Niño event warms the tropics and strengthens the Hadley circulation and subtropical jet (STJ). This phenomenon modifies the meridional circulation by diverting transient eddies to the north and south as a result of an anomalously low meridional wavenumber in the mid- and upper troposphere of the subtropics. These changes shift or weaken the polar front jet (PFJ; or eddy-driven jet) (Karoly 1989; Chen et al. 1996; Gallego et al. 2005; Carvalho et al. 2005) with direct impacts on high-latitude variables, such as sea ice (Rind et al. 2001; Yuan 2004; Pezza et al. 2012; Simpkins et al. 2012). Fogt and Bromwich (2006) showed that the ENSO teleconnection is amplified when the SAM is positively correlated with the Southern Oscillation index [SOI; strongest in September–October (SON) and December–February (DJF)], supported by evidence that the ENSO projects strongly onto the SAM in DJF (L'Heureux and Thompson 2006; Gregory and Noone 2008; Stammerjohn et al. 2008; Grainger et al. 2011; Cai et al. 2011). Fogt et al. (2011) showed that, when El Niño occurs with negative SAM (SAM−) events [or La Niña occurs with the positive SAM phase (SAM+)], strong circulation anomalies occur in the southeastern Pacific as a result of reinforcing anomalous transient eddy forcing. When these indices are out of phase, the regional circulation response is weakened because of interfering transient eddy processes. Thus, the internal variability associated with the SAM can impart a forcing on the high-latitude circulation that opposes the low-frequency forcing from the ENSO, but both impact SH circulation through the modulation of transient eddy momentum.

Ding et al. (2012) showed that the SAM is significantly correlated with tropical sea surface temperatures (SSTs) in the central Pacific Ocean during austral winter [June–August (JJA)] and spring (SON) and significantly correlated with eastern tropical Pacific SSTs during DJF. Other authors had already established the existence of ENSO "flavors" (e.g., Larkin and Harrison 2005; Ashok et al. 2007, 2009; Kug et al. 2009, 2010); that is, ENSO events may be classified by the location of their maximum heating/cooling in the tropical Pacific with distinct impacts on atmospheric circulation and climate. Central Pacific (CP) El Niños—also known as date line El Niños, ENSO Modoki, and warm pool–cold tongue events—have already been shown to be on the increase in recent decades compared to the classic warm tongue–eastern Pacific (EP) events (Ashok et al. 2007; Lee and McPhaden 2010). CP events lead to anomalous blocking over Australia associated with anomalous heating in the subtropics and a southward shift in the STJ in the eastern Pacific (Ashok et al. 2009). Lee et al. (2010) highlighted the 2009/10 CP event that coincided with a large anticyclonic anomaly in the south-central Pacific (SCP) during SON of that year, resulting in an anomalous northerly wind that brought warmer air and ocean water toward higher latitudes in this region. Kim et al. (2011) cited the nature of its decay phase and the strong anticyclone that was prevalent in the SCP in November (Lee et al. 2010). Reanalyses and models have shown that a distinct westward shift in the PSA pattern during JJA is also common in CP events (Sun et al. 2013; Ciasto et al. 2015), which impacts stationary eddies of heat and momentum (Wilson et al. 2014) associated with the Antarctic dipole (Yuan 2004) near the Antarctic Peninsula (AP).

Observation and modeling studies have revealed that the ENSO varies on a wide continuum of events, with each leading to different regional impacts (e.g., Capotondi 2013; Capotondi et al. 2015). A key task is figuring out how to improve the simulation of ENSO diversity in climate models. To do so, we need to know how well the models, both atmospheric and coupled models, are simulating the ENSO flavor events and their impacts in the high latitudes of the SH. While Wilson et al. (2014) focused on the changes to the stationary wave pattern, this work focuses on the transient eddies that are critical for ENSO and SAM modulation.

To achieve this task, we use an atmospheric model with prescribed global SSTs to simulate different El Niño flavors based on observed SSTs and evaluate their atmospheric circulation differences. Does the model provide robust signals that verify the dynamics, both in the zonal mean sense as well as specifically over the Pacific Ocean sector, as explained by previous research on the observed El Niño–SAM coupled forcing of high-latitude circulation (Seager et al. 2003; Fogt et al. 2011; Lim et al. 2013)? With the suggestion that the ratio of CP to EP events may increase in a warming world (Yeh et al. 2009), understanding the dynamics associated with each flavor may aid in improved modeling of such events to determine possible future climate implications. Section 2 explains the model characteristics, the El Niño and the SAM indices, and investigation methods. Section 3 verifies both the SAM and the El Niño influence on atmospheric circulation in the high latitudes, while section 4 provides an analysis of the eddy dynamics involved with their coupling. Section 5 explores these dynamics over the Pacific Ocean, with additional discussion and conclusions provided in section 6.

2. Data and methods

a. Numerical model

The Community Atmosphere Model (CAM), version 4 (Neale et al. 2010; Gent et al. 2011), the atmospheric component of the National Center for Atmospheric Research (NCAR) Community Climate System Model, is utilized, as sensitivity and idealized simulations have demonstrated it to be suitable for El Niño-flavor simulations (Wilson et al. 2014). This investigation tailors the lower boundary conditions [global SSTs and sea ice concentrations (SICs)] to match various observed El Niño events, which are prescribed using a dataset designed for uncoupled CAM simulations (Hurrell et al. 2008; available at http://cdp.ucar.edu/MergedHadleyOI). This dataset synthesizes the monthly mean Hadley Centre Sea Ice and SST dataset version 1.1 (HadISST1) (Rayner et al. 2003) with version 2 of the National Oceanic and Atmospheric Administration (NOAA) weekly Optimum Interpolation SST (OISSTv2) analysis (Reynolds et al. 2002). The CO_2 concentration and orbital parameters have been set to the observed 1990 values, and the standard stratospheric ozone has been used (Neale et al. 2010). The CAM radiation parameterization uses monthly mean ozone volume mixing ratios that are specified as a function of latitude, longitude, vertical pressure level, and time. Therefore, the three-dimensional stratospheric ozone structure is also annually repeating.

The spectral Eulerian dynamical core was used, which has 26 vertical levels and an 85-wave triangular truncation (T85L26, 128 × 256 gridpoint horizontal grid), with an equivalent resolution of 1.4°. This resolution allows the model to accurately represent eddies and their direct (and nonlinear) transports. The vertical structure is a hybrid coordinate system (Simmons and Strüfing 1981) that is terrain following near the earth's surface with a fixed upper boundary pressure surface (~3 hPa). Modifications to the convective momentum transport and a convective available potential energy dilution approximation have improved intraseasonal variability and weakened model trade winds, allowing for a better representation of ENSO (Hurrell et al. 2006; Neale et al. 2008).

b. CAM simulation strategy

The four main regions in the tropical Pacific Ocean monitored for the development of ENSO are as follows (from west to east): Niño-4 (5°N–5°S, 160°E–150°W); Niño-3.4 (5°N–5°S, 170°–120°W); Niño-3 (5°N–5°S, 150°–90°W); and Niño-1+2 (0°–10°S, 90°–80°W). Historically, the Niño-3.4 and Niño-3 regions have been used to identify anomalous SSTs above or below the climate base period (Trenberth 1997), but tropical Pacific SST anomalies are much more diverse and often not contained within a single predefined Niño region (e.g., Capotondi et al. 2015).

Figure 1 shows observed seasonal SST anomalies (w.r.t. 1981–2010) for five cases of El Niño selected for simulation with the CAM. The first two cases (1982/83 and 1997/98) are identified and organized in this study as EP events, with higher SST anomalies in the Niño-3 region than Niño-4. These events depict a warm tongue (anomalies >3°C) extending from the South American coast toward the central Pacific Ocean in response to the atmosphere–ocean interaction of weakening easterly trade winds and a deepening thermocline in the eastern Pacific. This allows warm SSTs from the warm pool region to move eastward, resulting in anomalous rising motion over the eastern tropical Pacific and anomalously sinking air in the warm pool region (vertical pressure velocity ω not shown). Despite their similarities, these two EP events demonstrated differences in their teleconnections, particularly to West Antarctica (Bromwich and Rogers 2000).

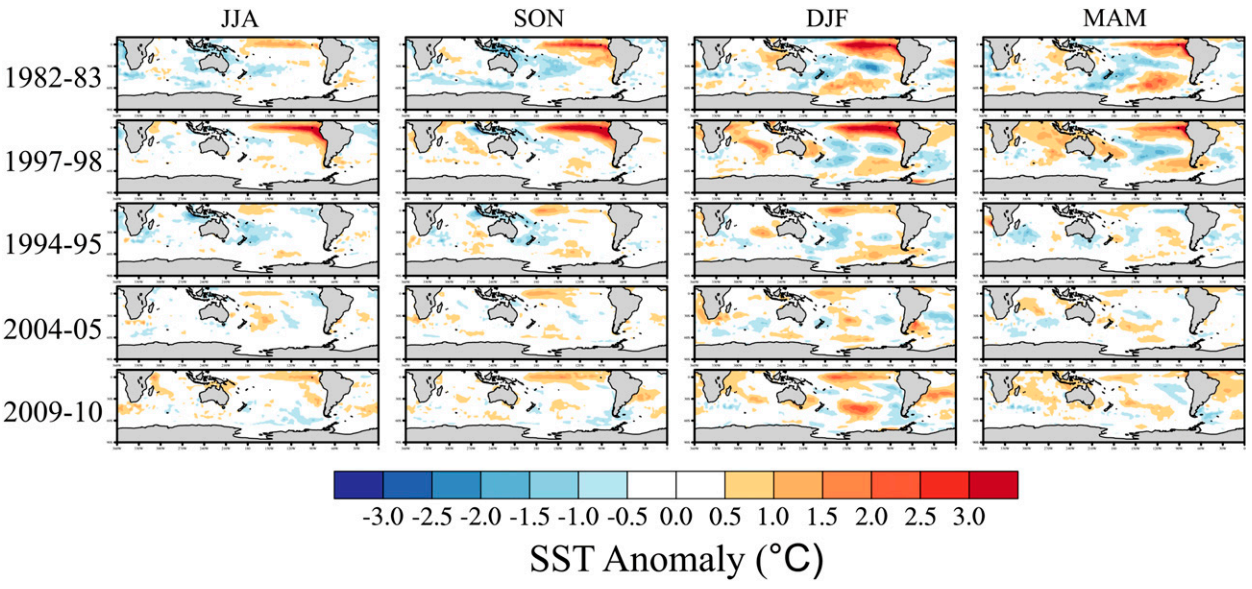

FIG. 1. (left)–(right) Seasonal SST anomalies (°C departure from 1981–2010 mean) for (top)–(bottom) the five El Niño-flavor simulations performed in this study.

The other three events (1994/95, 2004/05, and 2009/10) have been classified as CP events (e.g., Ashok et al. 2007; Kug et al. 2009; Lee et al. 2010). Spatially, these differ from their EP counterparts as SST anomalies form in the central Pacific Ocean during JJA but do not fully extend into the eastern Pacific basin (SST anomalies are greater in the Niño-4 region than in the Niño-3 region). For 1994/95 and 2004/05, the SST anomaly begins near the date line and is flanked by cool or neutral SST anomalies to the west and east (Fig. 1). This results in a small area of anomalous rising motion between 150°E–150°W and weak anomalous sinking motion on either side (ω not shown). The third CP event, 2009/10, bears some resemblance to an EP event in that, early in its development, the SST anomalies are concentrated in the eastern basin, but as the event developed further, the higher SST anomalies occurred in the Niño-4 region and were greater than the other two CP events. In fact, this was the strongest CP event since 1990 (defined as the Niño-4 index exceeding Niño-3) (McPhaden et al. 2011). We simulate this third event in order to capture more variability and in recognition of the potential to experience stronger CP events under global warming (Yeh et al. 2009). It should be noted that similar transient eddy behavior and anomalous circulation is found in each type of simulation, but events are composited here to increase confidence in the results.

Each CAM simulation was forced with cyclic (annually repeating) 12-month global SSTs and SICs based on each case (Fig. 1), and the CAM atmosphere freely responded to the specified sea surface conditions. The lower boundary conditions are based on the annual cycle from June of the year of development to May of the following year. This period was chosen in order to provide a smooth transition from the end of one annual cycle of tropical SST index to the next, as none of the cases show significant jumps between May and June in the repeated annual cycle. All model simulations begin in September (using the corresponding September SST and SIC values) and are run for 15 yr and 9 months, with the first 9 months discarded as spinup time. Though a longer period could have been selected, 15 yr was determined to provide an adequate number of ENSO–SAM events from which to draw robust conclusions. Finally, a control experiment with annually repeating SSTs and SICs (same as the El Niño simulations) based on climatological monthly SSTs and SICs for the period 1981–2010 was run and used to calculate all circulation anomalies for this study.

c. *Defining model SAM*

Not only has the SAM been defined as a hemispheric signal on various temporal scales (Ho et al. 2012), but it has also been described as a composition of regional patterns depending on the ocean basin of analysis (Ding et al. 2012), with regional impacts on local climate (e.g., Meneghini et al. 2007). We use the first (dominant mode) empirical orthogonal function (EOF) of the month-to-month field of 500-hPa geopotential height (Z500) anomalies (w.r.t. long-term monthly means of the control simulation) poleward of 10°S to define the SAM in each simulation. The monthly Z500 anomalies are weighted

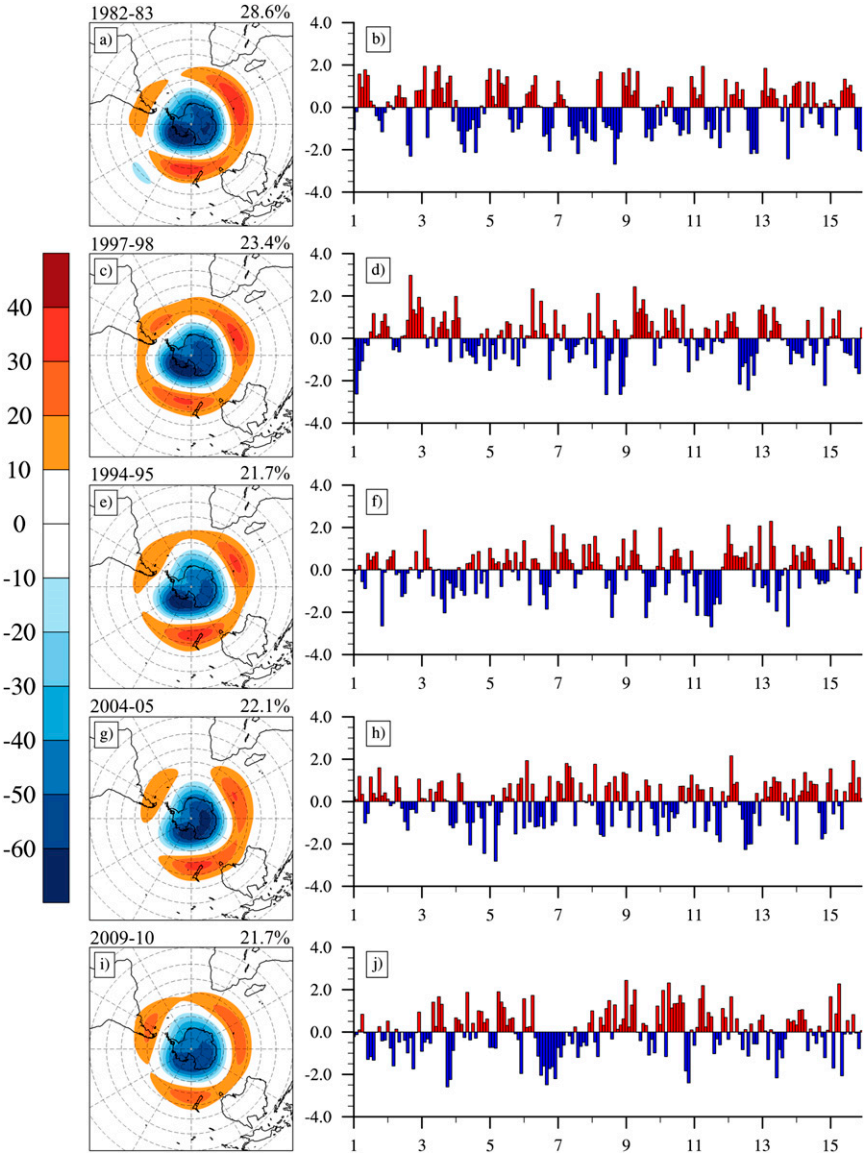

FIG. 2. (left) First rotated EOF patterns and (right) principal component indices representing the SAM in each El Niño simulation for (a),(b) 1982/83; (c),(d) 1997/98; (e),(f) 1994/95; (g),(h) 2004/05; and (i),(j) 2009/10.

by the square root of the cosine of the latitude in order to give area parity in the variances (Chung and Nigam 1999), with principal components constructed using the covariance matrix and varimax rotation (Richman 1986). The same method could be used with MSLP anomalies, but Z500 was chosen, as it represents the first major pressure level above the entire surface of Antarctica.

Figure 2 shows the first rotated EOF (REOF) modes from all five simulations as well as their SAM indices, which are constructed by projecting the monthly mean Z500 anomalies of each case onto their leading REOF modes and normalizing the time series by the standard deviations of the monthly indices for the entire 15-yr period. In all five cases, the first REOF mode is significantly separated from their respective REOF2 modes according to North et al.'s (1982) criteria. All simulations show a pattern consistent with the SAM from observations (e.g., Thompson and Wallace 2000; Fogt and Bromwich 2006), with structures of opposite signs between the mid- and high latitudes and 21.7%–28.6% of the variance of monthly Z500 variance explained. Despite the correlative nature of El Niño and the SAM (Ding et al. 2012), the internal variability is well maintained in CAM with both positive and negative phases of

SAM throughout the period. Correlation coefficients between the EP, CP, and EP versus CP SAM indices (except 1982/83 vs 1994/95) are not significant (at the $p < 0.05$ level). An additional test (not shown) was conducted using linear regression to remove the tropical-index-related variability from the Z500 anomalies at each grid point; then REOF analysis was performed on the residual Z500 anomaly field. The resulting EOF structures and variances were very similar to Fig. 2, and none of the composites were affected. These results support the idea that the internal variability of SAM modulates the impacts of the tropical teleconnections in the high southern latitudes (Fogt et al. 2011) regardless of flavor and is not merely induced by tropical variability.

The autocorrelation for each of the indices is shown in Fig. 3. All five simulations show significant autocorrelation at lag 1 (1 month), which is consistent with other studies (Ciasto and Thompson 2008; Gerber et al. 2008) as well as the Marshall index (Marshall 2003; Fig. 3f). The EP cases (Figs. 3a,b) demonstrate significant autocorrelation at longer lags compared to the CP cases. In particular, 1982/83 (Fig. 3a) shows significant autocorrelation at 1, 2, 4, 5, 6, 7, and 12 months. The sign of the autocorrelation also changes from positive to negative, most evident in the EP simulations but not significantly in 1994/95 (Fig. 3c) or 2004/05 (Fig. 3d) CP events. This is only weakly reflected in the Marshall SAM index (Fig. 3f) and likely reflects a model artifact as a result of the perpetual annual cycle of El Niño conditions present in the simulations (we forced a limited El Niño spectrum). Decreased autocorrelation at longer lags depicted by the CP events suggests that the tropical influence on the high latitudes is less robust with these types of events. However, the strong agreement between the simulated SAM indices and the Marshall index at shorter lags (the focus of this study) gives confidence that the SAM variability is well represented by the CAM.

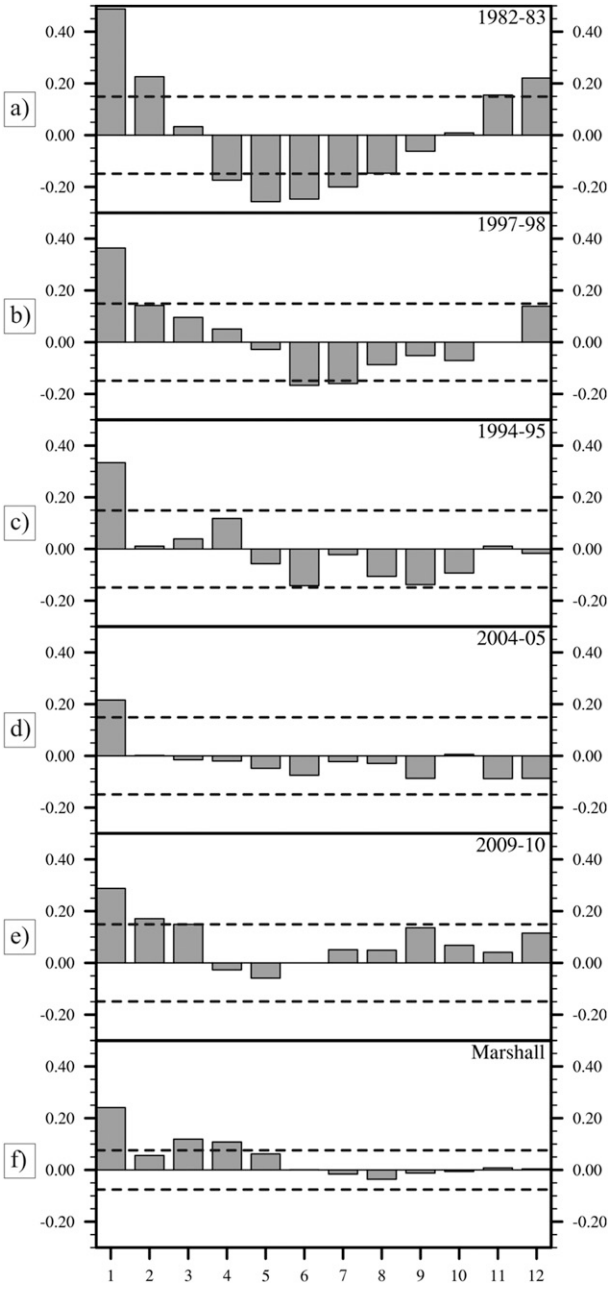

FIG. 3. Monthly autocorrelation for the SAM index for (a)–(e) all five El Niño simulations and (f) the Marshall index. The dashed lines represent the critical values for significance at $p < 0.05$.

3. Verification of simulated SAM modulation of the ENSO teleconnection

a. The importance of the SAM

To test whether CAM reproduces the in-phase and out-of-phase nature of the ENSO–SAM coupling on high southern latitude atmospheric circulation (Fogt et al. 2011), Fig. 4 shows the mean Z500 anomalies for September–December (SOND) for the 1997/98 (EP) and 2009/10 (CP) events (same results apply to the other simulations). While the SAM has been shown to be correlated with the central Pacific SST anomalies during JJA and the eastern Pacific SST anomalies during DJF (e.g., Ding et al. 2012; Lim et al. 2013), the focus in Fig. 4 is on the spring into early summer as the ENSO teleconnection has been demonstrated to be strongly correlated with the SAM during this season (Fogt and Bromwich 2006) and reflects a transition from asymmetric to more zonal flow (Karoly 1990). The European Centre for Medium-Range Weather Forecasts (ECMWF) interim reanalysis (ERA-Interim, hereafter ERAI; Dee et al. 2011) is used to compare September–December with the CAM simulations.

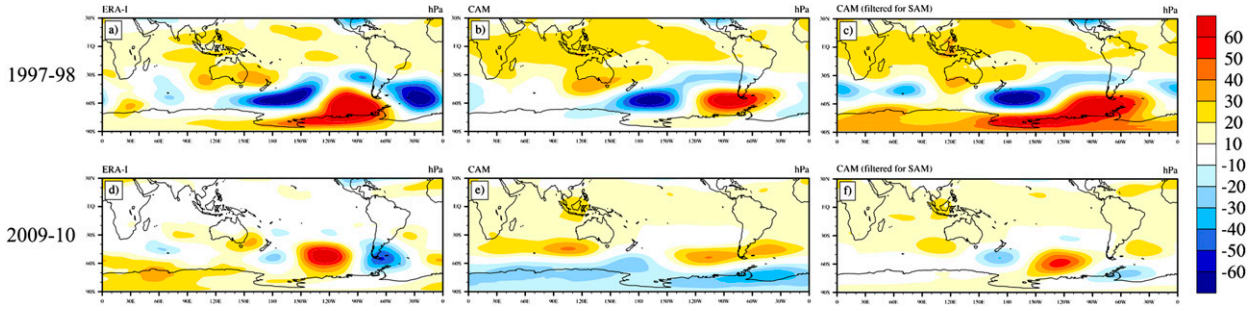

FIG. 4. Mean Z500 anomalies (hPa) for September–December for (top) 1997/98 and (bottom) 2009/10 for (a),(d) ERAI and (b),(e) CAM. For ERAI, the mean anomalies are the SOND 1997 departures from the 1981–2010 mean. For CAM, the mean anomalies are the mean 15 SOND departures from the control SOND mean. (e),(f) Mean anomalies for CAM where each month of the event has been filtered for the same SAM index that occurred during the actual event and inherent in the ERAI mean anomalies.

For the 1997/98 event, ERAI (Fig. 4a) shows the characteristic high-latitude response in the geopotential height field from the El Niño teleconnection with increased heights to the west of the AP representing atmospheric blocking that typically occurs there. In fact, the entire alternating wave train of Z500 anomalies, from the western Pacific across the South Pacific toward Antarctica is evident. CAM (Fig. 4b) shows a similar high-latitude signal in its Z500 anomalies with increased heights near the AP and lower heights near 60°S north of the Ross Sea. The response is less than that of ERAI, but it is important to note that this represents all 15 SOND seasons in the simulation regardless of other factors (specifically the SAM phase).

To assess whether CAM is adequately modeling the modulation of ENSO by the SAM, these 60 months (15 yr × 4-month period) are filtered for occurrences when the SAM index in CAM is the same phase that was observed. For the 1997 event, the SAM was neutral during September followed by the negative phase during October, November, and December. Once CAM events are filtered for the observed SAM phase (Fig. 4c), the response in the high southern latitudes is spatially more consistent with ERAI and stronger in magnitude. This supports the role the SAM plays in modulating the high-latitude response from El Niño to this region of the globe, as the anomalies are intensified when the SAM phases with the ENSO (specifically the SAM negative phase with El Niño in this example).

The importance of filtering for the SAM becomes even more apparent with the CP event. ERAI shows a different pattern of Z500 anomalies for the CP (2009/10) compared to the EP event (1997/98) (Fig. 4d). Geopotential heights increase (decrease) in the SCP (Drake Passage), consistent with the known shift in the stationary wave pattern across the SH. As Fig. 4e demonstrates, CAM does not fully reproduce the key features when considering the full 15-yr simulation. However, Fig. 4f reveals a more consistent response with ERAI, particularly in the SCP, when the phase of the SAM is considered. Observed SAM remained neutral from September through October, with a switch to the negative phase during November and December. Undoubtedly, the transition toward the negative SAM phase greatly supported the development of the large anticyclone during this particular November, as a low SAM signifies decreased zonal winds throughout the anticyclonic region (Lee et al. 2010). Figure 4 indicates that the high-latitude atmospheric circulation during ENSO events is forced by not only low-frequency ENSO variability but also by the internal variability of the SAM and must be considered when evaluating differences between EP and CP events.

b. *Compositing events*

Based on the monthly SAM indices in Fig. 2, 3-month running means were computed in order to obtain a seasonal SAM for all 3-month periods [JJA, July–September (JAS), August–October (ASO), SON, etc.]. Focus is on the four standard seasons from austral winter through autumn [JJA, SON, DJF, and March–May (MAM)]. Positive SAM (defined as >0.5) and negative SAM (defined as <-0.5) were identified for each season and simulation throughout the 15-yr period. The total number of events for each SAM phase (+ and −) for each type of El Niño flavor (EP and CP) and all seasons are shown in Table 1.

Several authors (e.g., Seager et al. 2003; Lim et al. 2013) have demonstrated that low-frequency El Niño variability can force a SAM− state through the modulation of the SH STJ that imparts a decrease in transient momentum flux convergence at high latitudes (weaker zonal flow) and an equatorward shift in the eddy-driven jet. While there is a tendency for such an occurrence, this does not necessarily mean a SAM− event will always occur with El Niño, as a number of recent observations prove otherwise (e.g., August–October 2013, November–December 2012, and June–September 2011). This primarily

TABLE 1. Counts of in-phase (SAM−) and out-of-phase (SAM+) seasonal events with EP and CP El Niños for each simulation and all seasons.

	JJA		SON		Phasing		DJF		MAM		Phasing	
	SAM−	SAM+	SAM−	SAM+	In phase	Out of phase	SAM−	SAM+	SAM−	SAM+	In phase	Out of phase
1982/83	2	5	2	9	4	14	8	2	7	2	15	4
1997/98	3	3	5	4	8	7	4	6	4	2	8	8
EP total	5	8	7	13	12	21	12	8	11	4	23	12
1994/95	3	7	2	5	5	12	5	2	4	4	9	6
2004/05	1	4	5	4	6	8	3	4	5	3	8	7
2009/10	4	4	1	5	5	9	5	4	4	2	9	6
CP total	8	15	8	14	16	29	13	10	13	9	26	19
Grand total	13	23	15	27	28	50	25	18	24	13	49	31

reflects the internal variability of the SAM, the influence of which on high-latitude circulation is well documented (e.g., Kidston et al. 2010; Fogt et al. 2011, 2012).

However, in-phase events (like El Niño–SAM−) tend to occur in November–February, and out-of-phase events occur in May–October (Fogt et al. 2011), a relationship further detailed through analysis of high-latitude ice cores (Schneider et al. 2012). Dynamically, it is proposed that the midlatitude jet in the SH is decoupled from changes in the tropics during JJA, specifically circulation changes associated with the Hadley cell (Lu et al. 2008; Barnes and Hartmann 2010). Table 1 supports this seasonal relationship in CAM for EP events with fewer in-phase events during JJA and SON and a greater number of in-phase events in DJF and MAM.

On the contrary, Lim et al. (2013) demonstrated a seasonal preference in the relationship between CP events and SAM− such that during JJA the southward displaced STJ increases westerlies on the poleward side of the STJ (30°–40°S). This southward shift in the STJ supports anomalous transient flux convergence in the midlatitudes while simultaneously decreasing westerly momentum in the higher latitudes (45°–65°S) and weakening the eddy-driven jet. However, CAM results in Table 1 do not support this seasonal preference with CP events, as fewer in-phase events occur in JJA similar to EP events. Wilson et al. (2014; cf. Fig. 6h therein) found an increase in westerlies on the poleward side of the STJ for their idealized intense CP El Niño, an indication that the tropical SST anomalies must be strong in order for the CAM to fully capture the tropical atmospheric forcing during these events.

Nevertheless, we composited the events in Table 1 in order to compare the dynamics associated with in-phase and out-of-phase events for both EP and CP events during JJA and DJF and assess whether the CAM is able to reproduce the observed response. By repeatedly forcing each type of event in CAM and compositing the events by SAM phasing (Fogt et al. 2011), model certainty and confidence in the dynamical mechanisms responsible for the atmosphere circulation variability increases. Using the results from section 3a, the remainder of this manuscript utilizes composites of in-phase and out-of-phase coupling between El Niño flavors and the SAM.

4. Simulated ENSO flavor dynamics

The ENSO and the SAM have been demonstrated to impact the zonal mean zonal wind, which can be represented by the following equation:

$$\frac{\partial[\overline{u}]}{\partial t} = -\left(\frac{[\overline{v}]}{a}\frac{\partial[\overline{u}]}{\partial\phi} + [\overline{\omega}]\frac{\partial[\overline{u}]}{\partial p}\right) + \left(f + \frac{[\overline{u}]\sin\phi}{a\cos\phi}\right)[\overline{v}] - \frac{1}{a\cos^2\phi}\frac{\partial}{\partial\phi}([\overline{u}^*\overline{v}^*]\cos^2\phi) - \frac{\partial}{\partial p}[\overline{u}^*\overline{\omega}^*] - \frac{1}{a\cos^2\phi}\frac{\partial}{\partial\phi}([\overline{u'v'}]\cos^2\phi) - \frac{\partial}{\partial p}[\overline{u'\omega'}] - \overline{D[u]}, \quad (1)$$

where u is the zonal wind, v is the meridional wind, ω is the vertical pressure velocity, a is the radius of the earth, ϕ is latitude, p is pressure, f is the Coriolis parameter, $\overline{D[u]}$ is damping (i.e., friction), square brackets indicate zonal means, asterisks indicate departures from zonal means, overbars signify monthly means, and primes indicate departures from monthly means (Seager et al. 2003). The first term on the right-hand side is the advection of zonal wind by the mean meridional circulation, the second term is the Coriolis torque, the third and fourth terms are associated with the momentum flux convergence of stationary waves (not addressed in this manuscript), and the fifth and sixth terms are the forcing of momentum flux convergence by transient eddies. Figure 5 shows composite mean mass streamfunction and overturning circulation for El Niño-flavor SAM− events. Figure 6 depicts anomalous zonal mean zonal wind, anomalous meridional circulation, and resultant

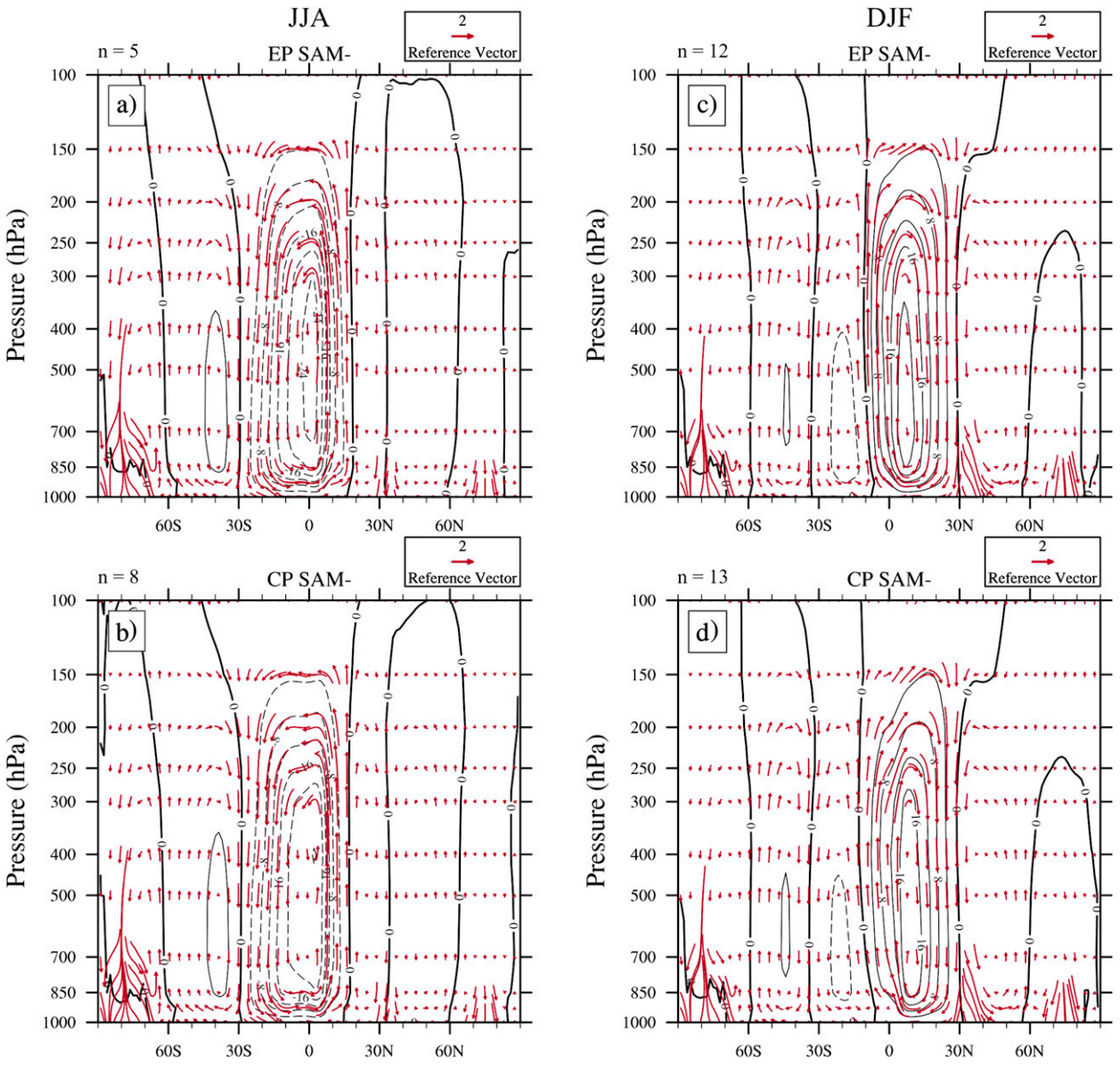

FIG. 5. Composite mean mass streamfunction (10^9 kg s^{-1}) and meridional circulation vectors (red arrows; v in m s^{-1} and w in mm s^{-1}) for (a),(b) JJA and (c),(d) DJF during in-phase events: (top) EP SAM− and (bottom) CP SAM−. The total number of cases (n) for each type of event from Table 1 is noted for each composite.

Coriolis torque, while Fig. 7 illustrates anomalous transient eddy momentum fluxes and convergence (as in Fogt et al. 2011). These anomalies were calculated w.r.t. the long-term monthly means of the control simulation and composited for each combination of El Niño and SAM with results from JJA and DJF displayed in the figures.

a. JJA

For in-phase events in CAM during JJA (Figs. 5a,b), the descending branch of the Hadley cell is located in the SH with sinking motion between the equator (EQ) and 30°S. Figure 6a shows anomalous sinking motion between EQ and 10°S but anomalous rising motion between 15°–30°S for the EP–SAM− composite, indicating a stronger Hadley circulation that is contracted toward the equator (Seager et al. 2003; Lim et al. 2013). As a result, the zonal mean zonal wind is anomalously strong between EQ and 10°S, demonstrating a strengthened STJ that is shifted equatorward. The CP–SAM− composite (Fig. 5b) shows a less vigorous Hadley circulation than the EP–SAM− composite (Fig. 5a), though still slightly stronger than the control simulation (not shown). Though stronger

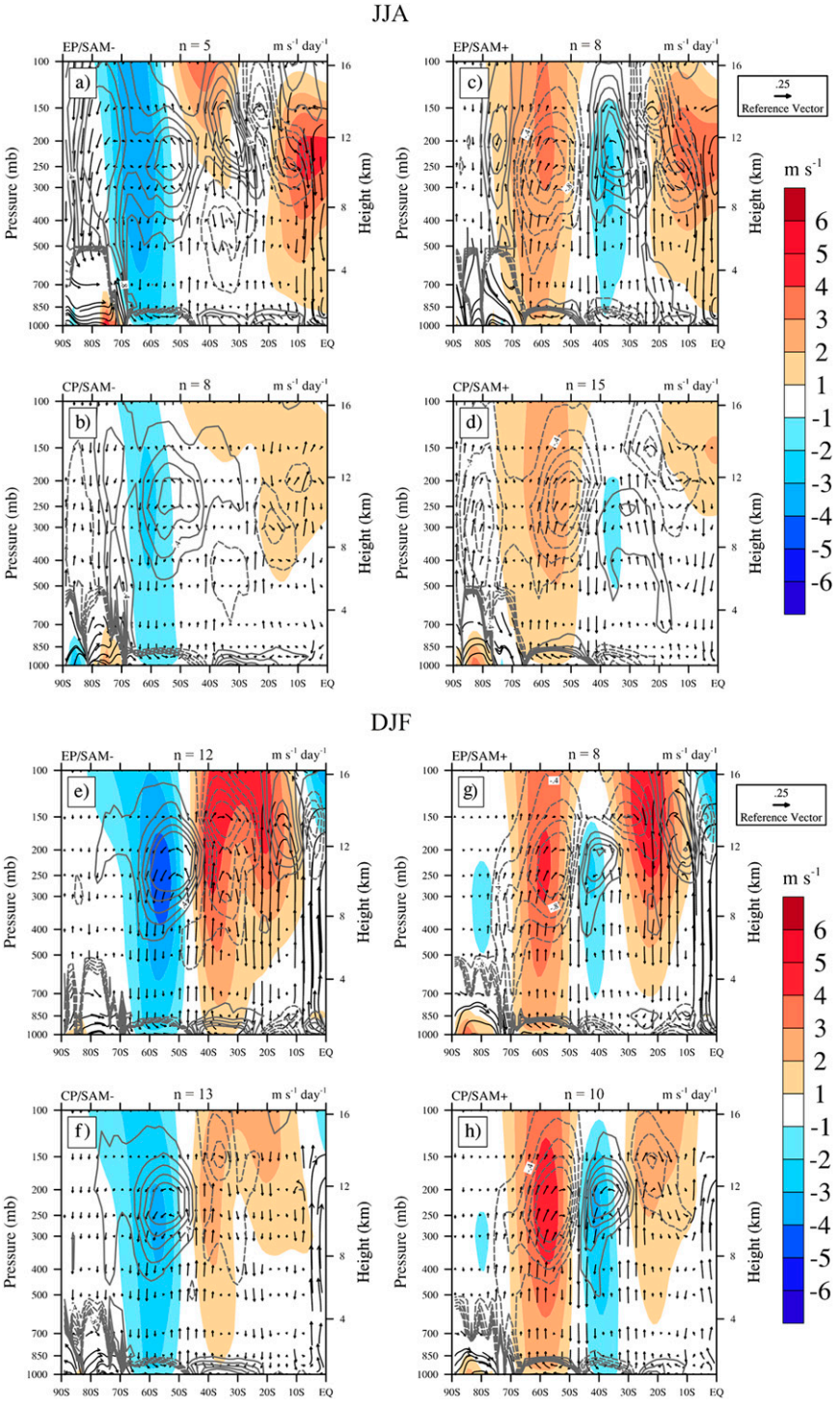

FIG. 6. Anomalous zonal mean zonal wind ($m\,s^{-1}$; color shaded), anomalous meridional circulation vectors (black arrows; v in $m\,s^{-1}$ and w in $mm\,s^{-1}$), and resultant Coriolis torque ($m\,s^{-1}\,day^{-1}$; contoured by 0.2; zero removed) during (a)–(d) JJA and (e)–(h) DJF for (a),(e) EP–SAM−; (b),(f) CP–SAM−; (c),(g) EP–SAM+; and (d),(h) CP–SAM+. The total number of cases (n) for each type of event from Table 1 is noted for each composite.

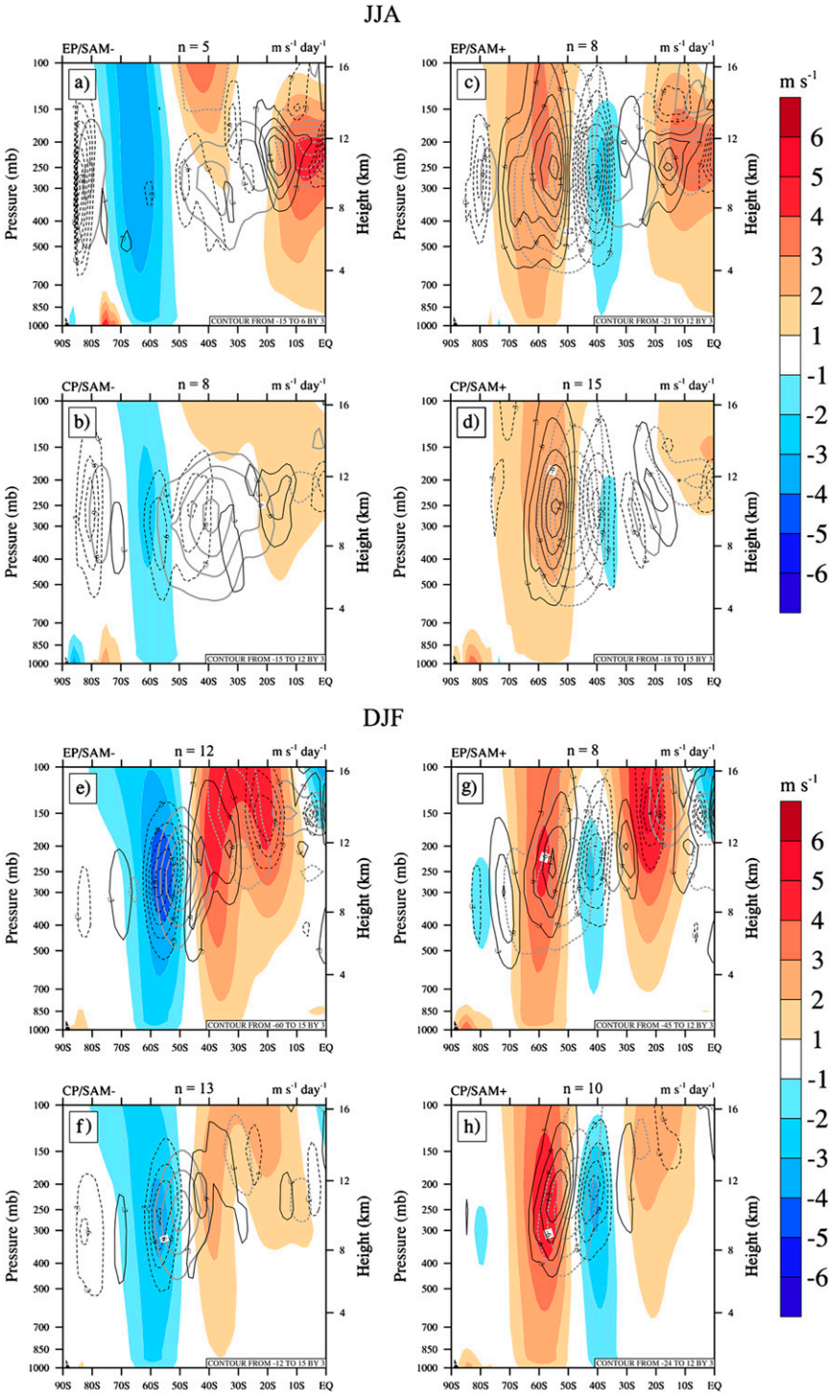

FIG. 7. As in Fig. 6, but with vectors and Coriolis torque replaced by anomalous meridional transient eddy momentum flux ($m^2 s^{-2}$; gray contours; solid for equatorward; dashed for poleward) and anomalous transient momentum flux convergence ($m s^{-1} day^{-1}$; black contours; solid for convergence; dashed for divergence). The transient eddy momentum fluxes have been cosine weighted (as in Seager et al. 2003; Fogt et al. 2011) and are contoured every $3 m^2 s^{-2}$, and the convergence is contoured every $0.3 m s^{-1} day^{-1}$. The zero contours have been removed.

than the control (1–2 m s^{-1}), the CP–SAM− STJ is weaker than in EP–SAM− (~3 m s^{-1}) and shifted slightly south (Figs. 6a,b).

Both EP–SAM− and CP–SAM− composites show weaker zonal mean zonal wind between 50°–70°S and primarily anomalous sinking motion poleward of 70°S as well, consistent with Fogt et al. (2011). For JJA in-phase events (Figs. 7a,b), anomalous equatorward flux centered near 40°S (solid gray contours) generates transient eddy momentum convergence on the equatorward side (between 10°–20°S) that helps maintain the stronger STJ (Seager et al. 2003; Lim et al. 2013). On the poleward side of the center of anomalous equatorward flux (between 40° and 60°S), transient eddy momentum divergence (black dashed contours) is present, more apparent in the CP–SAM− case, which acts as a weakening force on westerly momentum and helps shift the eddy-driven jet equatorward. This forcing is in opposition to the Coriolis torque (gray contours; positive in Figs. 6a,b) that must be overcome in order for the zonal mean zonal wind anomalies to be maintained (Thompson and Wallace 2000; Seager et al. 2003; L'Heureux and Thompson 2006; Fogt et al. 2011).

As discussed in section 3, Lim et al. (2013) demonstrated a dynamical mechanism for CP events during JJA when shifts in the eddy-driven jet are thought to be decoupled from variations of the STJ and the Hadley cell under EP-type regimes (Lu et al. 2008). The anomalous equatorward flux (solid gray contours) is greater in the CP–SAM− composite (Fig. 7b) compared to the EP–SAM− composite (Fig. 7a), with stronger transient eddy divergence between 50° and 60°S. However, there does not appear to be a significant increase in westerlies on the poleward side of the STJ in the CP–SAM− composite as in Wilson et al. (2014).

For the out-of-phase events, both composites reflect a strong Hadley circulation in the tropics (not shown) that is similar to the in-phase events in Figs. 5a,b. Again, the anomalous sinking motion between EQ and 10°S is much stronger in the EP–SAM+ composite than CP–SAM+ composite (Figs. 6c,d). The tropical influence still promotes a strengthened STJ in the low latitudes of both composites. Zonal mean zonal wind anomalies are negative between 30° and 40°S, a reflection of the poleward shift in the eddy-driven jet and resultant changes in the anomalous transient eddy momentum convergence–divergence. This change to the zonal wind velocity stimulates positive Coriolis torque (gray solid contours), indicating a change in midlatitude eddy behavior compared to SAM− events (Figs. 6a,b). This is apparent in Fig. 7c where anomalous poleward transient eddy flux centered near 50°S and anomalous equatorward flux centered near 35°S result in transient eddy momentum divergence (negative forcing on the zonal mean zonal wind) between 30° and 40°S. Although this phenomenon is present in the CP–SAM+ case (Figs. 6d and 7d), the anomalous transient flux divergence and the zonal mean zonal wind are of lesser magnitudes.

In the high latitudes, EP–SAM+ and CP–SAM+ (Figs. 6c,d) show positive zonal mean wind anomalies concentrated between 50° and 70°S, which are consistent with reanalysis results for El Niño–SAM+ events (Fogt et al. 2011). Rising motion between 58° and 72°S in the EP–SAM+ case and between 52° and 65°S in the CP–SAM+ case is also consistent with observations of a strong thermally direct polar cell, the rising motion of which is dynamically driven by the divergence of meridional winds aloft that are induced by the westerly momentum convergence peaking between 50° and 60°S and westerly momentum divergence in higher latitudes (Figs. 7c,d) (Thompson and Wallace 2000; Fogt et al. 2011; Kidston et al. 2010; Hendon et al. 2014). In summary, differences in CP composites compared to EP are generally twofold during JJA: (i) weaker zonal mean zonal wind anomalies and (ii) weaker meridional circulation. However, the feedback between the transient eddies and the mean flow is stronger in the CP composites than the EP composites, supporting the findings of Lim et al. (2013), who show a poleward shift of the STJ causes anomalous convergence of the eddy momentum flux on the equatorward side of the eddy-driven jet, which helps shift the eddy-driven jet equatorward. These results suggest that the tropical forcing in the CAM on zonal wind anomalies is less robust in the CP cases than in the EP cases, likely because of the weaker magnitudes of the tropical SST anomalies in CP events, even during JJA, when CP cases may be more likely to occur (Lim et al. 2013).

b. DJF

The anomalous zonal mean zonal wind anomalies and meridional circulation are much stronger in DJF (Figs. 6e–h) than in JJA (Figs. 6a–d), and their patterns are consistent with reanalyses (Fogt et al. 2011). CAM results suggest a more robust tropical forcing on SH circulation during this season. The SH part of the rising branch of the Hadley cell circulation is located between EQ and 10°S (Figs. 5c,d) and is anomalously strong in both EP and CP composites regardless of the SAM phase (Figs. 6e,f). Once again, EP events in CAM demonstrate a greater modulation of the Hadley circulation as anomalous rising motion near the EQ is much stronger in the EP–SAM− composite (Fig. 6e) than the CP–SAM− composite (Fig. 6f). The STJ is stronger in both the EP–SAM− and CP–SAM− events (2–5 m s^{-1}) compared to the control and 1–2 m s^{-1} stronger in the EP–SAM− composite than the CP–SAM− composite.

The larger changes (positive and negative) to the zonal mean zonal wind also intensify the transient eddy momentum flux anomalies, as these peak in DJF as well (Figs. 7e–h). Anomalously weak (strong) zonal mean zonal wind anomalies are centered near 60°S, associated with in-phase (out of phase) events. The anomalous equatorward momentum flux centers (gray solid contours) are now located near 50°S in the EP–SAM− (Fig. 7e) and CP–SAM− (Fig. 7f) and are stronger in the EP–SAM− than CP–SAM− composite. Interestingly, the DJF CP–SAM− equatorward flux during DJF (Fig. 7f) is weaker ($\sim 3\,m^2\,s^{-2}$) compared to JJA (Fig. 7b), which dynamically supports a weaker relationship between CP events and the SAM during DJF. EP events, however, are more dynamically conducive during DJF, as an intensified and contracted STJ helps maintain an equatorward-shifted eddy-driven jet by shifting the transient eddy momentum convergence equatorward in support of the low phase of the SAM (e.g., Seager et al. 2003; L'Heureux and Thompson 2006; Fogt et al. 2011; Lim et al. 2013).

For the EP–SAM+ (Fig. 6g) and CP–SAM+ (Fig. 6h) composites, rising motion poleward of 60°S and anomalous positive zonal mean zonal wind anomalies indicate that the SAM+ forcing on the high-latitude flow is strong enough to overcome the tropical forcing transmitted through the SH from El Niño. This stresses the importance that the anomalous flow in the high latitudes is not only forced by tropical variability but is modulated by the internal variability inherently associated with the SAM through the baroclinicity-driven PFJ. While the zonal mean zonal wind anomalies in the tropics are weaker for the in-phase CP composite compared to the EP case, the positive zonal mean zonal wind anomalies in the high latitudes in the out-of-phase CP–SAM+ are slightly stronger than the EP–SAM+ which demonstrates a weakened opposing force present during CP events compared to the EP type.

Figures 7g and 7h demonstrate anomalous poleward fluxes near 50°S that lead to anomalous transient eddy convergence near 60°S and positive zonal mean zonal wind anomalies that are associated with SAM+. The magnitude of anomalous poleward transient eddy momentum fluxes in the CP–SAM+ composite is similar to the EP–SAM+ composite, but the pattern is more compact. This shows greater transient eddy momentum convergence near 55°S and stronger zonal mean zonal wind anomalies near 60°S. This too demonstrates that SAM modulates the El Niño forcing, as weaker CP events are not able to dynamically interfere with (through changes in the transient eddy momentum fluxes) the strong westerly momentum inherent during SAM+ events.

Thus, CAM results support the intensification of circulation anomalies associated with the interaction between SAM− events and El Niño, and there is modeling support that their dynamics differ between seasons. The strongest impacts are realized during EP–SAM− events in DJF when in-phase events are more likely to occur (Fogt et al. 2011; Lim et al. 2013). Still, dynamically CP events impart a similar upper-level forcing on transient momentum in the high latitudes during JJA because of a southward shift in the STJ that supports weakened westerlies in the high latitudes during this season. On the other hand, SAM+ conditions interfere with transient eddy behavior in the midlatitudes during both flavors of El Niño, limiting the efficiency to which the tropically induced transient eddy momentum may propagate and reach the high latitudes (Fogt et al. 2011). This supports conclusions drawn by Barnes and Hartmann (2010, 2012) that, as the high-latitude jet moves poleward, waves are unlikely to break on the poleward flank of the jet. Instead, they turn and propagate equatorward, breaking at critical lower latitudes.

5. Regional dynamics over the Pacific Ocean

Knowing that the ENSO signal is predominantly propagated to the high southern latitudes via wave activity and the modulation of jet streams over the Pacific Ocean, Chen et al. (1996) determined that the balance between mean flow momentum convergence and ageostrophic flow (pressure gradient and Coriolis torque) determines the variation of the STJ, while transient eddy momentum convergence is largely responsible for changes in the PFJ. Fogt et al. (2011) demonstrated mutual modulations of transient eddy momentum fluxes from both ENSO and the SAM, with in-phase (e.g., El Niño–SAM−) events leading to transient eddy anomalies from each that amplify resultant circulation anomalies—supported by the full zonal mean perspective presented in section 4. With these results in mind, focus is given to the transient eddy dynamics involved in the El Niño teleconnection and the SAM modulation under different flavors in CAM specifically over the Pacific Ocean. Similar to Fogt et al. (2011), the local $\mathbf{E}_u$ vector formulation of Trenberth (1986, 1991) is used, which is similar in concept to a localized Eliassen–Palm (E–P) flux (Edmon et al. 1980). The zonal component of the $\mathbf{E}_u$ vector is given by $(1/2)(\overline{v'^2} - \overline{u'^2})$, while the meridional component is the negative of the transient eddy momentum flux $-\overline{u'v'}$. The $\mathbf{E}_u$ vector points in the direction of the group velocity and its divergence represents a westerly wind forcing (Trenberth 1991).

Figures 8a,b and 8e,f show anomalous zonal mean zonal wind and anomalous meridional transient eddy momentum flux (similar to Fig. 7 without transient eddy momentum flux convergence) during JJA and

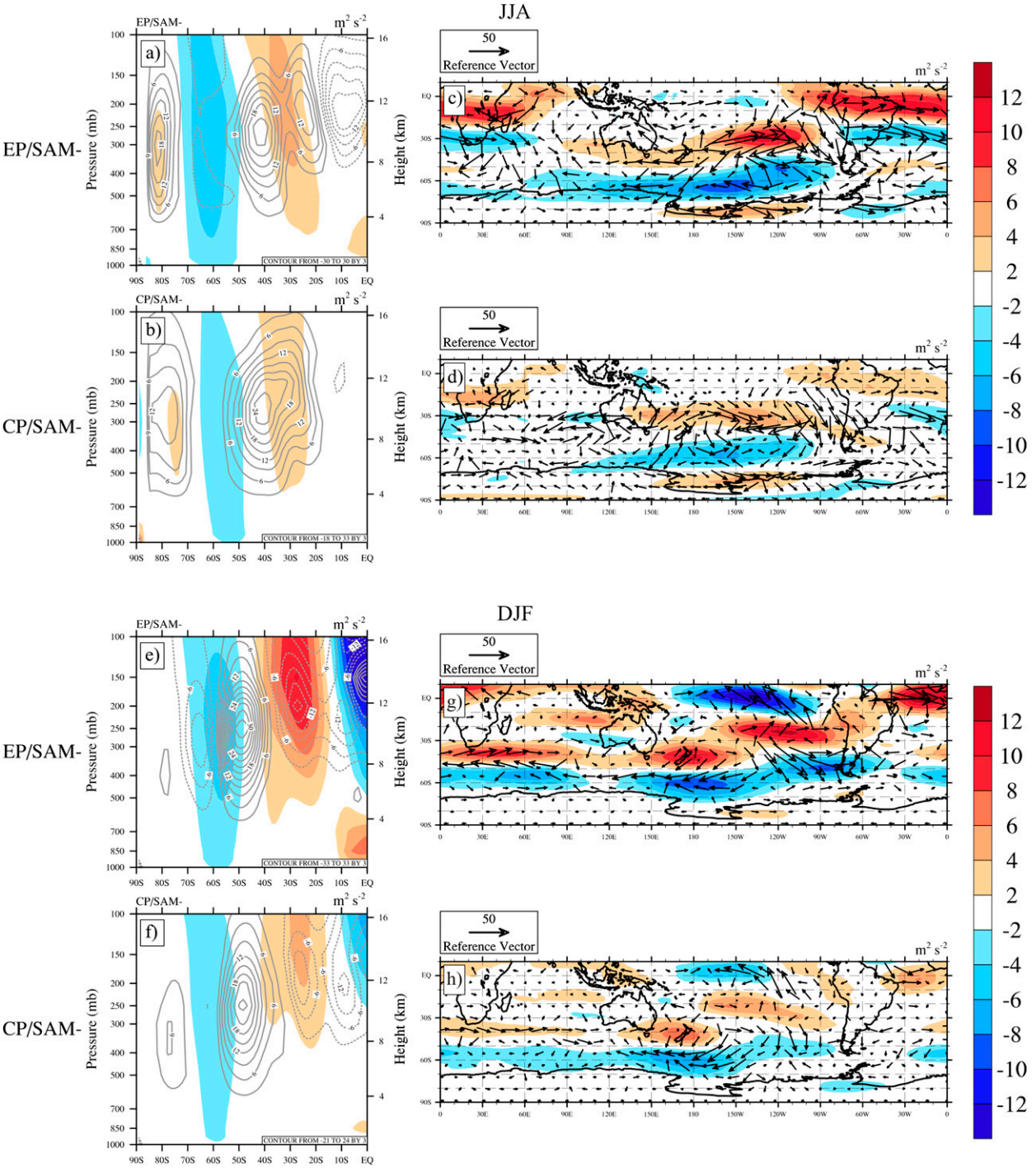

FIG. 8. (left) Anomalous zonal mean zonal wind ($m\,s^{-1}$; color shaded) and anomalous meridional transient eddy momentum flux ($m^2\,s^{-2}$; gray contours; solid for equatorward; dashed for poleward) during (a),(b) JJA and (e),(f) DJF averaged for the Pacific sector (160°E–60°W) for (a),(e) EP–SAM− and (b),(f) CP–SAM−. The transient eddy momentum fluxes have been cosine weighted (as in Seager et al. 2003; Fogt et al. 2011) and are contoured every $3\,m^2\,s^{-2}$. The zero contours have been removed. (right) Anomalous mean zonal wind ($m\,s^{-1}$; color shaded) and $\mathbf{E}_u$ vectors at 300 hPa for (c),(g) EP–SAM− and (d),(h) CP–SAM− shown for JJA and DJF, respectively.

DJF, respectively, averaged for the Pacific sector (160°E–60°W). Overall, the patterns and impacts on the zonal mean zonal wind are similar for both EP–SAM− and CP–SAM− composites during JJA, but anomalous equatorward transient eddy momentum fluxes (gray contours) are centered near 40°S and are much stronger over the Pacific Ocean sector than the full zonal mean (Figs. 7a,b). This corresponds to greater transient eddy momentum convergence on the poleward side of the STJ (not shown), resulting in transient eddy momentum divergence near 50°S and negative zonal wind anomalies near 60°S. Note the transient eddy momentum flux is stronger in the CP–SAM− case (Fig. 8b) than the EP–SAM− case (Fig. 8a) during JJA, when CP events are more likely to support SAM− events (Lim et al. 2013). Again, the structure is similar for both types of El Niño flavors, but the anomalous dynamics are stronger in CP events despite less impact in the CAM on the zonal mean zonal wind.

Anomalous mean zonal wind and $\mathbf{E}_u$ vectors at 300 hPa are shown are for JJA (Figs. 8c,d) and DJF (Figs. 8g,h), respectively. Overall, the $\mathbf{E}_u$ vectors are much stronger over the Pacific than the rest of the SH, similar to the findings by Fogt et al. (2011). Figures 8c and 8d show divergence of the local $\mathbf{E}_u$ vectors between 20° and 40°S and 150° and 90°W, which represents the addition of westerly momentum to the intensified STJ [note the anomalously strong anomalous mean zonal wind (red shading in this area)] in both El Niño composites compared to the control simulation. The divergence of the $\mathbf{E}_u$ vectors is more intense in the EP–SAM− than CP–SAM− composite, which is reflected by the greater mean zonal wind anomalies. Conversely, convergence of $\mathbf{E}_u$ vectors in higher latitudes represents a negative forcing on the westerly flow, with negative zonal wind anomalies between 50° and 70°S throughout most of the South Pacific.

For DJF, the center of anomalous equatorward transient eddy momentum flux shifts to 50°S in both composites (Figs. 8e,f), reflecting the SAM variability and the deepening circumpolar trough, with very strong transient eddy momentum flux divergence near 60°S (not shown) near the core of negative zonal wind anomalies. Again, the CP–SAM− negative composite shows weaker dynamics and zonal mean zonal wind anomalies than the EP–SAM− composite for this season. Figure 8g shows strong convergence of local $\mathbf{E}_u$ vectors in the South Pacific, leading to weaker mean zonal wind (blue shading). While the magnitude of the poleward wave activity toward the high latitudes ($\mathbf{E}_u$ vectors point in the direction of the wave activity) is stronger, equatorward wave activity from higher-to-lower latitudes is still evident between 60° and 70°S and 120° and 90°W) (Fig. 8g). Also, CP–SAM− poleward $\mathbf{E}_u$ vectors (Fig. 8h) from the low latitudes toward the high latitudes are weaker, yet the stronger equatorward $\mathbf{E}_u$ vectors emanating from the Southern Ocean (60°–70°S, 120°–90°W) toward lower latitudes indicate once again that the forcing associated with the SAM on weaker zonal flow is actively participating in the modulation.

6. Conclusions

In this paper, we have simulated several EP and CP El Niño events with the CAM using prescribed sea surface conditions, focusing on the dynamics associated with each and their interaction with the high southern latitudes. The results of this study confirm that the CAM captures well the spatial and temporal variability of atmospheric circulation associated with the SAM and its modulation of the El Niño teleconnection to Antarctica. Correctly modeling SAM variability is necessary for accurate anomalous circulation in the high southern latitudes associated with El Niño, especially for the CP events that only resemble ERAI when the correct SAM phase occurs in the model. These results allow us to composite in-phase (El Niño–SAM−) and out-of-phase (El Niño–SAM+) events for both EP and CP cases and analyze the seasonal differences in their dynamics.

While Wilson et al. (2014) confirmed westward shifts in the PSA pattern during CP events that impact circulation in the high southern latitudes (Sun et al. 2013; Ciasto et al. 2015), this analysis focuses on the transient eddy dynamics associated with El Niño-flavor variability. As in observations, a distinct seasonal preference emerges from the model, with EP in-phase (out of phase) events more likely to occur during DJF (JJA). Intense westerly wind anomalies associated with a strong STJ during DJF leads to anomalous equatorward momentum flux on the equatorward side of the eddy-driven jet, shifting this jet equatorward, consistent with the low phase of the SAM (e.g., Seager et al. 2003; L'Heureux and Thompson 2006; Fogt et al. 2011; Lim et al. 2013). Feedback between the transient eddies and the mean flow is stronger in the CP composites than the EP composites during JJA, supporting the findings of Lim et al. (2013), who show a poleward shift of the STJ during this season causes anomalous convergence of the eddy momentum flux on the equatorward side of the eddy-driven jet, which also drives the PFJ northward.

For out-of-phase cases during both seasons, the El Niño–associated teleconnection to the high southern latitudes is strongly modulated by the SAM behavior, as a strong eddy-driven jet is well maintained by high-latitude transient eddy convergence despite the tropical forcing. A regional view shows that the zonal mean anomalies are much greater over the Pacific sector, responding to much greater transient eddy momentum

flux and convergence. However, the process is the same: a co-forcing response from both an intensification of tropically induced stronger STJ as well as additional transient eddy activity (equatorward wave activity) associated with high-latitude forcing.

Certainly, this analysis has taken advantage of the well-maintained internal variability in the CAM. However, there is evidence that the CAM does not fully capture the tropical forcing of anomalous high-latitude circulation. For instance, correlations between the tropical SST indices and the SAM indices in the model are generally low and insignificant. The zonal mean zonal wind anomalies associated with the STJ in the CP simulations are not as strongly modulated as those in the EP simulations, even during JJA, likely because of the relative differences in EP versus CP SST anomalies (much larger in EP events). Likewise, the model simulations in this study have a first-order depiction of stratospheric ozone behavior, which along with limitations to the stratosphere–troposphere coupling (Gerber and Polvani 2009), represent an area of improvement for future model simulations of this type.

Moreover, other factors contribute to the complexity of atmospheric circulation around Antarctica, particularly in the South Pacific Ocean, including the Atlantic multidecadal oscillation (Li et al. 2014) and the Pacific decadal oscillation (Clem and Fogt 2015; Goodwin et al. 2016). Seasonal and annual mean sea ice trends around Antarctica are significantly positive over the last 35 yr (to a lesser degree during DJF) and are largely consistent with long-term trends in MSLP (Simmonds 2015). In fact, a negative trend in the MSLP during JJA just north of the ice edge between 60° and 120°W—which helps maintain the regional sea ice anomalies between the Amundsen–Bellingshausen Seas and the Ross Sea—may also reflect the influence of CP El Niño events (less blocking in the southeastern Pacific with anticyclonic anomalies in the south-central Pacific). Discerning how the interactions among these many processes evolve under changing El Niño regimes will be important for understanding the climate changes that have occurred and for modeling future changes of the Antarctic environment.

Acknowledgments. This research was supported by the National Science Foundation (NSF) Grants ATM-0751291 and PLR-1341695. CAM simulations were conducted using the Ohio Supercomputer Center's (https://www.osc.edu/) IBM Cluster 1350 (Glenn Cluster). The authors thank the three anonymous reviewers for their insightful critiques and suggestions.

REFERENCES

Arkin, P. A., 1982: The relationship between interannual variability in the 200 mb tropical wind field and the Southern Oscillation. *Mon. Wea. Rev.*, **110**, 1393–1404, doi:10.1175/1520-0493(1982)110<1393:TRBIVI>2.0.CO;2.

Ashok, K., S. K. Behera, S. A. Rao, H. Weng, and T. Yamagata, 2007: El Niño Modoki and its possible teleconnection. *J. Geophys. Res.*, **112**, C11007, doi:10.1029/2006JC003798.

——, C.-Y. Tam, and W.-J. Lee, 2009: ENSO Modoki impact on the Southern Hemisphere storm track activity during extended austral winter. *Geophys. Res. Lett.*, **36**, L12705, doi:10.1029/2009GL038847.

Baldwin, M. P., 2001: Annular modes in global daily surface pressure. *Geophys. Res. Lett.*, **28**, 4115–4118, doi:10.1029/2001GL013564.

Barnes, E. A., and D. L. Hartmann, 2010: Dynamical feedbacks of the southern annular mode in winter and summer. *J. Atmos. Sci.*, **67**, 2320–2330, doi:10.1175/2010JAS3385.1.

——, and ——, 2012: Detection of Rossby wave breaking and its response to shifts of the midlatitude jet with climate change. *J. Geophys. Res.*, **117**, D09117, doi:10.1029/2012JD017469.

Bromwich, D. H., and A. N. Rogers, 2000: The El Niño–Southern Oscillation modulation of West Antarctic precipitation. *West Antarctic Ice Sheet: Behavior and Environment*, R. B. Alley and R. A. Bindschadler, Eds., Antarctic Research Series, Vol. 77, Amer. Geophys. Union, 91–103, doi:10.1029/AR077.

Cai, W. J., A. Sullivan, and T. Cowan, 2011: Interactions of ENSO, the IOD, and the SAM in CMIP3 models. *J. Climate*, **24**, 1688–1704, doi:10.1175/2010JCLI3744.1.

Capotondi, A., 2013: ENSO diversity in the NCAR CCSM4 climate model. *J. Geophys. Res.*, **118**, 4755–4770, doi:10.1002/jgrc.20335.

——, and Coauthors, 2015: Understanding ENSO diversity. *Bull. Amer. Meteor. Soc.*, **96**, 921–938, doi:10.1175/BAMS-D-13-00117.1.

Carvalho, L. M. V., C. Jones, and T. Ambrizzi, 2005: Opposite phases of the Antarctic Oscillation and relationships with intraseasonal to interannual activity in the tropics during austral summer. *J. Climate*, **18**, 702–718, doi:10.1175/JCLI-3284.1.

Chen, B., S. R. Smith, and D. H. Bromwich, 1996: Evolution of the tropospheric split jet over the South Pacific Ocean during the 1986–89 ENSO cycle. *Mon. Wea. Rev.*, **124**, 1711–1731, doi:10.1175/1520-0493(1996)124<1711:EOTTSJ>2.0.CO;2.

Chung, C., and S. Nigam, 1999: Weighting of geophysical data in principal component analysis. *J. Geophys. Res.*, **104**, 16 925–16 928, doi:10.1029/1999JD900234.

Ciasto, L. M., and D. W. J. Thompson, 2008: Observations of large-scale ocean–atmosphere interaction in the Southern Hemisphere. *J. Climate*, **21**, 1244–1259, doi:10.1175/2007JCLI1809.1.

——, G. R. Simpkins, and M. H. England, 2015: Teleconnections between tropical Pacific SST anomalies and extratropical Southern Hemisphere climate. *J. Climate*, **28**, 56–65, doi:10.1175/JCLI-D-14-00438.1.

Clem, K. R., and R. L. Fogt, 2015: South Pacific circulation changes and their connection to the tropics and regional Antarctic warming in austral spring, 1979–2012. *J. Geophys. Res. Atmos.*, **120**, 2773–2792, doi:10.1002/2014JD022940.

Dee, D. P., and Coauthors, 2011: The ERA-Interim reanalysis: Configuration and performance of the data assimilation system. *Quart. J. Roy. Meteor. Soc.*, **137**, 553–597, doi:10.1002/qj.828.

Ding, Q., E. J. Steig, D. S. Battisti, and J. M. Wallace, 2012: Influence of the tropics on the southern annular mode. *J. Climate*, **25**, 6330–6348, doi:10.1175/JCLI-D-11-00523.1.

Edmon, H. J., B. J. Hoskins, and M. E. McIntyre, 1980: Eliassen–Palm flux cross sections for the troposphere. *J. Atmos. Sci.*, **37**, 2600–2616, doi:10.1175/1520-0469(1980)037<2600:EPCSFT>2.0.CO;2.

Fogt, R. L., and D. H. Bromwich, 2006: Decadal variability of the ENSO teleconnection to the high-latitude South Pacific governed by coupling with the southern annular mode. *J. Climate*, **19**, 979–997, doi:10.1175/JCLI3671.1.

——, ——, and K. Hines, 2011: Understanding the SAM influence on the South Pacific ENSO teleconnection. *Climate Dyn.*, **36**, 1555–1576, doi:10.1007/s00382-010-0905-0.

——, A. J. Wovrosh, R. A. Langen, and I. Simmonds, 2012: The characteristic variability and connection to the underlying synoptic activity of the Amundsen–Bellingshausen Seas Low. *J. Geophys. Res.*, **117**, D07111, doi:10.1029/2011JD017337.

Fyfe, J. C., G. J. Boer, and G. M. Flato, 1999: The Arctic and Antarctic oscillations and their projected changes under global warming. *Geophys. Res. Lett.*, **26**, 1601–1604, doi:10.1029/1999GL900317.

Gallego, D., P. Ribera, R. Garcia-Herrera, E. Hernandez, and L. Gimeno, 2005: A new look for the Southern Hemisphere jet stream. *Climate Dyn.*, **24**, 607–621, doi:10.1007/s00382-005-0006-7.

Gent, P. R., and Coauthors, 2011: The Community Climate System Model version 4. *J. Climate*, **24**, 4973–4991, doi:10.1175/2011JCLI4083.1.

Gerber, E. P., and L. M. Polvani, 2009: Stratosphere–troposphere coupling in a relatively simple AGCM: The importance of stratospheric variability. *J. Climate*, **22**, 1920–1933, doi:10.1175/2008JCLI2548.1.

——, ——, and D. Ancukiewicz, 2008: Annular mode time scales in the Intergovernmental Panel on Climate Change Fourth Assessment Report models. *Geophys. Res. Lett.*, **35**, L22707, doi:10.1029/2008GL035712.

Gillett, N. P., and D. W. J. Thompson, 2003: Simulation of recent Southern Hemisphere climate change. *Science*, **302**, 273–275, doi:10.1126/science.1087440.

Gong, D., and S. Wang, 1999: Definition of Antarctic Oscillation index. *Geophys. Res. Lett.*, **26**, 459–462, doi:10.1029/1999GL900003.

Goodwin, B. P., E. Mosley-Thompson, A. B. Wilson, S. E. Porter, and M. R. Sierra-Hernandez, 2016: Accumulation variability in the Antarctic Peninsula: The role of large-scale atmospheric oscillations and their interactions. *J. Climate*, doi:10.1175/JCLI-D-15-0354.1, in press.

Grainger, S., and Coauthors, 2011: Modes of variability of Southern Hemisphere atmospheric circulation estimated by AGCMs. *Climate Dyn.*, **36**, 473–490, doi:10.1007/s00382-009-0720-7.

Gregory, S., and D. Noone, 2008: Variability in the teleconnection between the El Niño–Southern Oscillation and West Antarctic climate deduced from West Antarctic ice core isotope records. *J. Geophys. Res.*, **113**, D17110, doi:10.1029/2007JD009107.

Hall, A., and M. Visbeck, 2002: Synchronous variability in the Southern Hemisphere atmosphere, sea ice, and ocean resulting from the annular mode. *J. Climate*, **15**, 3043–3057, doi:10.1175/1520-0442(2002)015<3043:SVITSH>2.0.CO;2.

Harangozo, S. A., 2004: The relationship of Pacific deep tropical convection to the winter and springtime extratropical atmospheric circulation of the South Pacific in El Niño events. *Geophys. Res. Lett.*, **31**, L05206, doi:10.1029/2003GL018667.

Hartmann, D. L., and F. Lo, 1998: Wave-driven flow vacillation in the Southern Hemisphere. *J. Atmos. Sci.*, **55**, 1303–1315, doi:10.1175/1520-0469(1998)055<1303:WDZFVI>2.0.CO;2.

Hendon, H. H., E.-P. Lim, and H. Nguyen, 2014: Seasonal variations of subtropical precipitation associated with the southern annular mode. *J. Climate*, **27**, 3446–3460, doi:10.1175/JCLI-D-13-00550.1.

Ho, M., A. S. Kiem, and D. C. Verdon-Kidd, 2012: The southern annular mode: A comparison of indices. *Hydrol. Earth Syst. Sci.*, **16**, 967–982, doi:10.5194/hess-16-967-2012.

Hoskins, B. J., and D. J. Karoly, 1981: The steady linear response of a spherical atmosphere to thermal and orographic forcing. *J. Atmos. Sci.*, **38**, 1179–1196, doi:10.1175/1520-0469(1981)038<1179:TSLROA>2.0.CO;2.

Hurrell, J. W., J. J. Hack, A. S. Phillips, J. Caron, and J. Yin, 2006: The dynamical simulation of the Community Atmosphere Model version 3 (CAM3). *J. Climate*, **19**, 2162–2183, doi:10.1175/JCLI3762.1.

——, ——, D. Shea, J. M. Caron, and J. Rosinski, 2008: A new sea surface temperature and sea ice boundary dataset for the Community Atmosphere Model. *J. Climate*, **21**, 5145–5153, doi:10.1175/2008JCLI2292.1.

Karoly, D. J., 1989: Southern Hemisphere circulation features associated with El Niño–Southern Oscillation events. *J. Climate*, **2**, 1239–1252, doi:10.1175/1520-0442(1989)002<1239:SHCFAW>2.0.CO;2.

——, 1990: The role of transient eddies in low-frequency zonal variations of the Southern Hemisphere circulation. *Tellus*, **42A**, 41–50, doi:10.1034/j.1600-0870.1990.00005.x.

Kidson, J. W., 1999: Principal modes of Southern Hemisphere low-frequency variability obtained from NCEP–NCAR reanalyses. *J. Climate*, **12**, 2808–2830, doi:10.1175/1520-0442(1999)012<2808:PMOSHL>2.0.CO;2.

Kidston, J., D. M. W. Frierson, J. A. Renwick, and G. K. Vallis, 2010: Observations, simulations, and dynamics of jet stream variability and annular modes. *J. Climate*, **23**, 6186–6199, doi:10.1175/2010JCLI3235.1.

Kiladis, G. N., and K. C. Mo, 1998: Interannual and intraseasonal variability in the Southern Hemisphere. *Meteorology of the Southern Hemisphere*, *Meteor. Monogr.*, No. 49, Amer. Meteor. Soc., 307–336, doi:10.1007/978-1-935704-10-2_11.

Kim, W., S.-W. Yeh, J.-H. Kim, J.-S. Kug, and M. Kwon, 2011: The unique 2009–2010 El Niño event: A fast phase transition of warm pool El Niño to La Niña. *Geophys. Res. Lett.*, **38**, L15809, doi:10.1029/2011GL048521.

Kug, J.-S., F.-F. Jin, and S.-I. An, 2009: Two types of El Niño events: Cold tongue El Niño and warm pool El Niño. *J. Climate*, **22**, 1499–1515, doi:10.1175/2008JCLI2624.1.

——, J. Choi, S.-I. An, F.-F. Jin, and A. T. Wittenberg, 2010: Warm pool and cold tongue El Niño events as simulated by the GFDL 2.1 coupled GCM. *J. Climate*, **23**, 1226–1239, doi:10.1175/2009JCLI3293.1.

Kushner, P. J., I. M. Held, and T. L. Delworth, 2001: Southern Hemisphere atmospheric circulation response to global warming. *J. Climate*, **14**, 2238–2249, doi:10.1175/1520-0442(2001)014<0001:SHACRT>2.0.CO;2.

Lachlan-Cope, T., and W. Connolley, 2006: Teleconnections between the tropical Pacific and the Amundsen–Bellingshausen Seas: Role of the El Niño–Southern Oscillation. *J. Geophys. Res.*, **111**, D23101, doi:10.1029/2005JD006386.

Larkin, N. K., and D. E. Harrison, 2005: Global seasonal temperature and precipitation anomalies during El Niño autumn and winter. *Geophys. Res. Lett.*, **32**, L16705, doi:10.1029/2005GL022860.

Lee, T., and M. J. McPhaden, 2010: Increasing intensity of El Niño in the central-equatorial Pacific. *Geophys. Res. Lett.*, **37**, L14603, doi:10.1029/2010GL044007.

——, and Coauthors, 2010: Record warming in the South Pacific and western Antarctica associated with the strong central-Pacific El Niño in 2009–10. *Geophys. Res. Lett.*, **37**, L19704, doi:10.1029/2010GL044865.

L'Heureux, M. L., and D. W. J. Thompson, 2006: Observed relationships between the El Niño–Southern Oscillation and the

extratropical zonal-mean circulation. *J. Climate*, **19**, 276–287, doi:10.1175/JCLI3617.1.

Li, X., D. M. Holland, E. P. Gerber, and C. Yoo, 2014: Impacts of the north and tropical Atlantic Ocean on the Antarctic Peninsula and sea ice. *Nature*, **505**, 538–542, doi:10.1038/nature12945.

Lim, E.-P., H. H. Hendon, and H. Rashid, 2013: Seasonal predictability of the southern annular mode due to its association with ENSO. *J. Climate*, **26**, 8037–8054, doi:10.1175/JCLI-D-13-00006.1.

Limpasuvan, V., and D. L. Hartmann, 1999: Eddies and the annular modes of climate variability. *Geophys. Res. Lett.*, **26**, 3133–3136, doi:10.1029/1999GL010478.

——, and ——, 2000: Wave-maintained annular modes of climate variability. *J. Climate*, **13**, 4414–4429, doi:10.1175/1520-0442(2000)013<4414:WMAMOC>2.0.CO;2.

Lu, J., G. Chen, and D. M. W. Frierson, 2008: Response of the zonal mean atmospheric circulation to El Niño versus global warming. *J. Climate*, **21**, 5835–5851, doi:10.1175/2008JCLI2200.1.

Marshall, G. J., 2003: Trends in the southern annular mode from observations and reanalyses. *J. Climate*, **16**, 4134–4143, doi:10.1175/1520-0442(2003)016<4134:TITSAM>2.0.CO;2.

——, P. A. Stott, J. Turner, W. M. Connolley, J. C. King, and T. A. Lachlan-Cope, 2004: Causes of exceptional atmospheric circulation changes in the Southern Hemisphere. *Geophys. Res. Lett.*, **31**, L14205, doi:10.1029/2004GL019952.

McPhaden, M. J., T. Lee, and D. McClurg, 2011: El Niño and its relationship to changing background conditions in the tropical Pacific. *Geophys. Res. Lett.*, **38**, L15709, doi:10.1029/2011GL048275.

Meneghini, B., I. Simmonds, and I. N. Smith, 2007: Association between Australian rainfall and the Southern Annular Mode. *Int. J. Climatol.*, **27**, 109–121, doi:10.1002/joc.1370.

Mo, K. C., and M. Ghil, 1987: Statistics and dynamics of persistent anomalies. *J. Atmos. Sci.*, **44**, 877–902, doi:10.1175/1520-0469(1987)044<0877:SADOPA>2.0.CO;2.

——, and J. N. Peagle, 2001: The Pacific–South American modes and their downstream effects. *Int. J. Climatol.*, **21**, 1211–1229, doi:10.1002/joc.685.

Neale, R. B., J. H. Richter, and M. Jochum, 2008: The impact of convection on ENSO: From a delayed oscillator to a series of events. *J. Climate*, **21**, 5904–5924, doi:10.1175/2008JCLI2244.1.

——, and Coauthors, 2010: Description of the NCAR Community Atmosphere Model (CAM 4.0). NCAR Tech. Note NCAR/TN-485+STR, 212 pp. [Available online at http://www.cesm.ucar.edu/models/ccsm4.0/cam/docs/description/cam4_desc.pdf.]

North, G. R., T. L. Bell, and R. F. Cahalan, 1982: Sampling errors in the estimation of empirical orthogonal functions. *Mon. Wea. Rev.*, **110**, 699–706, doi:10.1175/1520-0493(1982)110<0699:SEITEO>2.0.CO;2.

Pezza, A. B., H. A. Rashid, and I. Simmonds, 2012: Climate links and recent extremes in Antarctic sea ice, high-latitude cyclones, Southern Annular Mode and ENSO. *Climate Dyn.*, **38**, 57–73, doi:10.1007/s00382-011-1044-y.

Rashid, H. A., and I. Simmonds, 2004: Eddy–zonal flow interactions associated with the Southern Hemisphere annular mode: Results from NCEP–DOE reanalysis and a quasi-linear model. *J. Atmos. Sci.*, **61**, 873–888, doi:10.1175/1520-0469(2004)061<0873:EFIAWT>2.0.CO;2.

——, and ——, 2005: Southern Hemisphere annular mode variability and the role of optimal nonmodal growth. *J. Atmos. Sci.*, **62**, 1947–1961, doi:10.1175/JAS3444.1.

Rayner, N. A., D. E. Parker, E. B. Horton, C. K. Folland, L. V. Alexander, D. P. Rowell, E. C. Kent, and A. Kaplan, 2003: Global analyses of sea surface temperature, sea ice, and night marine air temperature since the late nineteenth century. *J. Geophys. Res.*, **108**, 4407, doi:10.1029/2002JD002670.

Renwick, J. A., 1998: ENSO-related variability in the frequency of South Pacific blocking. *Mon. Wea. Rev.*, **126**, 3117–3123, doi:10.1175/1520-0493(1998)126<3117:ERVITF>2.0.CO;2.

——, and M. J. Revell, 1999: Blocking over the South Pacific and Rossby wave propagation. *Mon. Wea. Rev.*, **127**, 2233–2247, doi:10.1175/1520-0493(1999)127<2233:BOTSPA>2.0.CO;2.

Revell, M. J., J. W. Kidson, and G. N. Kiladis, 2001: Interpreting low-frequency modes of Southern Hemisphere atmospheric variability as the rotational response to divergent forcing. *Mon. Wea. Rev.*, **129**, 2416–2425, doi:10.1175/1520-0493(2001)129<2416:ILFMOS>2.0.CO;2.

Reynolds, R. W., N. A. Rayner, T. M. Smith, D. C. Stokes, and W. Wang, 2002: An improved in situ and satellite SST analysis for climate. *J. Climate*, **15**, 1609–1625, doi:10.1175/1520-0442(2002)015<1609:AIISAS>2.0.CO;2.

Richman, M. B., 1986: Rotation of principal components. *Int. J. Climatol.*, **6**, 293–335, doi:10.1002/joc.3370060305.

Rind, D., M. Chandler, J. Lerner, D. G. Martinson, and X. Yuan, 2001: Climate response to basin-specific changes in latitudinal temperature gradients and implications for sea ice variability. *J. Geophys. Res.*, **106**, 20 161–20 173, doi:10.1029/2000JD900643.

Rogers, J. C., and H. van Loon, 1982: Spatial variability of sea level pressure and 500-mb height anomalies over the Southern Hemisphere. *Mon. Wea. Rev.*, **110**, 1375–1392, doi:10.1175/1520-0493(1982)110<1375:SVOSLP>2.0.CO;2.

Schneider, D. P., Y. Okumura, and C. Deser, 2012: Observed Antarctic interannual climate variability and tropical linkages. *J. Climate*, **25**, 4048–4066, doi:10.1175/JCLI-D-11-00273.1.

Seager, R., N. Harnik, Y. Kushnir, W. Robinson, and J. Miller, 2003: Mechanisms of hemispherically symmetric climate variability. *J. Climate*, **16**, 2960–2978, doi:10.1175/1520-0442(2003)016<2960:MOHSCV>2.0.CO;2.

Sen Gupta, A., and M. H. England, 2006: Coupled ocean–atmosphere–ice response to variations in the southern annular mode. *J. Climate*, **19**, 4457–4486, doi:10.1175/JCLI3843.1.

Simmonds, I., 2015: Comparing and contrasting the behaviour of Arctic and Antarctic sea ice over the 35 year period 1979–2013. *Ann. Glaciol.*, **56**, 18–28, doi:10.3189/2015AoG69A909.

——, and J. C. King, 2004: Global and hemispheric climate variations affecting the Southern Ocean. *Antarct. Sci.*, **16**, 401–413, doi:10.1017/S0954102004002226.

Simmons, A. J., and R. Strüfing, 1981: An energy and angular-momentum conserving finite-difference scheme, hybrid coordinates and medium-range weather prediction. ECMWF Tech. Rep. 28, 68 pp.

Simpkins, G. R., and A. Y. Karpechko, 2012: Sensitivity of the southern annular mode to greenhouse gas emission scenarios. *Climate Dyn.*, **38**, 563–572, doi:10.1007/s00382-011-1121-2.

——, L. M. Ciasto, D. W. J. Thompson, and M. H. England, 2012: Seasonal relationships between large-scale climate variability and Antarctic sea ice concentration. *J. Climate*, **25**, 5451–5469, doi:10.1175/JCLI-D-11-00367.1.

Stammerjohn, S. E., D. G. Martinson, R. C. Smith, X. Yuan, and D. Rind, 2008: Trends in Antarctic annual sea ice retreat and advance and their relation to El Niño–Southern Oscillation and Southern Annular Mode variability. *J. Geophys. Res.*, **113**, C03S90, doi:10.1029/2007JC004269.

Sun, D., F. Xue, and T. Zhou, 2013: Impact of two types of El Niño on atmospheric circulation in the Southern Hemisphere. *Adv. Atmos. Sci.*, **30**, 1732–1742, doi:10.1007/s00376-013-2287-9.

Thompson, D. W. J., and J. M. Wallace, 2000: Annular modes in the extratropical circulation. Part I: Month-to-month variability. *J. Climate*, **13**, 1000–1016, doi:10.1175/1520-0442(2000)013<1000:AMITEC>2.0.CO;2.

——, and S. Solomon, 2002: Interpretation of recent Southern Hemisphere climate change. *Science*, **296**, 895–899, doi:10.1126/science.1069270.

——, ——, P. J. Kushner, M. H. England, K. M. Grise, and D. J. Karoly, 2011: Signatures of the Antarctic ozone hole in Southern Hemisphere surface climate change. *Nat. Geosci.*, **4**, 741–749, doi:10.1038/ngeo1296.

Trenberth, K. E., 1986: An assessment of the impact of transient eddies on the zonal mean flow during a blocking episode using localized Eliassen–Palm flux diagnostics. *J. Atmos. Sci.*, **43**, 2070–2087, doi:10.1175/1520-0469(1986)043<2070:AAOTIO>2.0.CO;2.

——, 1991: Storm tracks in the Southern Hemisphere. *J. Atmos. Sci.*, **48**, 2159–2178, doi:10.1175/1520-0469(1991)048<2159:STITSH>2.0.CO;2.

——, 1997: The definition of El Niño. *Bull. Amer. Meteor. Soc.*, **78**, 2771–2777, doi:10.1175/1520-0477(1997)078<2771:TDOENO>2.0.CO;2.

Wilson, A. B., D. H. Bromwich, K. M. Hines, and S.-H. Wang, 2014: El Niño flavors and their simulated impacts on atmospheric circulation in the high southern latitudes. *J. Climate*, **27**, 8934–8955, doi:10.1175/JCLI-D-14-00296.1.

Yeh, S.-W., J.-S. Kug, B. Dewitte, M.-H. Kwon, B. P. Kirtman, and F.-F. Jin, 2009: El Niño in a changing climate. *Nature*, **461**, 511–514, doi:10.1038/nature08316.

Yu, J.-Y., and D. L. Hartmann, 1993: Zonal flow vacillation and eddy forcing in a simple GCM of the atmosphere. *J. Atmos. Sci.*, **50**, 3244–3259, doi:10.1175/1520-0469(1993)050<3244:ZFVAEF>2.0.CO;2.

Yuan, X., 2004: ENSO-related impacts on Antarctic sea ice: A synthesis of phenomenon and mechanisms. *Antarct. Sci.*, **16**, 415–425, doi:10.1017/S0954102004002238.

Zheng, F., J. Li, R. T. Clark, and H. C. Nnamchi, 2013: Simulation and projection of the Southern Hemisphere Annular Mode in CMIP5 models. *J. Climate*, **26**, 9860–9879, doi:10.1175/JCLI-D-13-00204.1.